



Synthesis, Characterization of rGO/CoZrO₃ and rGO/Nd₂Zr₂O₇ nanocomposite for the application of Photocatalytic and Antimicrobial Activity

Mathivanan Nallathambi a, Krishnasamy Kuppusamy a *

a, a * Department of Chemistry, Annamalai University, Annamalainagar
Chidambaram, Tamilnadu, India, mail: krishnasamybala56@gmail.com.

ABSTRACT

Reduced graphene oxide wrapped cobalt and neodymium based zirconium oxide nanocomposites were synthesized via facile hydrothermal method. The synthesized rGO/CoZrO₃ and rGO/Nd₂Zr₂O₇ nanocomposites were characterized by various analytical techniques such as XRD, FT-IR, SEM, XPS and UV-DRS analysis. The phase and crystalline size of rGO, ZrO₂, CoZrO₃, Nd₂Zr₂O₇, rGO/CoZrO₃ and rGO/Nd₂Zr₂O₇ are found to be 26.5, 30.2, 38.7, 44.0, 40.3 and 48.6 nm respectively and morphology were examined by using SEM which revealed that rGO/CoZrO₃ and rGO/Nd₂Zr₂O₇ exhibited as aggregated flakes nanoparticles are uniformly distributed over the surface of rGO with a 2D sheet structure. The band gap was calculated using UV-DRS analysis and the band gap of rGO/CoZrO₃ and rGO/Nd₂Zr₂O₇ was found to be 3.6 and 3.2 eV respectively. The synthesized rGO/CoZrO₃ and rGO/Nd₂Zr₂O₇ nanocomposites are used as catalysts for photocatalytic degradation of methylene blue dye with the degradation efficiency of 88.2% and as active anti-bacterial materials and the results revealed that the synthesized rGO/CoZrO₃ and rGO/Nd₂Zr₂O₇ exhibited excellent photodegradation and antimicrobial properties. This research outcome might be useful to propose the lead material for photodegradation and antimicrobial pathogens.

Keywords: Graphene, Zirconium oxide, Neodymium oxide, Hydrothermal, Photocatalytic and Anti-bacterial.

Received 23.07.2023

Revised 21.08.2023

Accepted 13.09.2023

Introduction

Metallic nanocomposites include rGO/CoZrO₃ and rGO/Nd₂Zr₂O₇ materials are synthesized via hydrothermal, microemulsion, electrochemical and laser pyrolysis processes[1]. The chemical process that produces the most nanocomposites among them is probably hydrothermal, which is also the simplest and most effective.

There is a strong incentive to discover novel bactericides from diverse sources since the emergence of new bacterial strains that are resistant to existing antibiotics has become a difficult issue for public health[2]. Recent developments in nanotechnology have offered appealing ways to synthesis alternative antimicrobial agents and decrease biofilm formation [3]. The prepared nanomaterials of rGO/CoZrO₃ and rGO/Nd₂Zr₂O₇ have been used as catalyst for photocatalytic degradation to reduce water pollution. Although a variety of bacteria have recently been identified to be very toxic to nanoparticles, relatively little is known about how poisonous rGO/CoZrO₃ and rGO/Nd₂Zr₂O₇ nanocomposites are to these microorganisms [4]. In the current study, an effort has been made to synthesize rGO/CoZrO₃ and rGO/Nd₂Zr₂O₇ using a hydrothermal method and are characterized using XRD, FT-IR, SEM, XPS and UV-DRS. Photocatalytic degradation with methylene blue dye and antibacterial activity against four human pathogenic Gram-positive and Gram-negative bacteria have been investigated.

MATERIAL AND METHODS

Materials

In this study the required chemicals such as graphite powder, sodium nitrate, sulphuric acid, potassium permanganate, zirconyl nitrate, cobalt chloride, oxalic acid and hydrogen peroxide were in the analytical grade and used as such without any further purification.

Synthesis of Graphene Oxide

Graphene Oxide was synthesized by modified Hummer's method. 46ml of H₂SO₄ and 1g of graphite powder and NaNO₃, were taken in the beaker and the solution was stirring for one hour for 500 rpm. 6g of KMnO₄

was added slowly and the solution was stirred half an hour in ice bath condition [5]. Further, 50 ml of water was added drop wise, and cooling the prearrangement in room temperature, then the arrangement was warming at 100 °C and 10ml of H₂O₂ was added for the formation of graphene oxide.

Synthesis of Reduced Graphene Oxide

400 mg of powdered GO was dissolved in 20 ml of water and 10 ml of hydrazine hydrate was added and it used as a reducing agent to reduce the graphene oxide[6]. The mixture was centrifuged at 4000 r/s for 40 minutes after being put on a magnetic stirrer for 30 minutes at 60 °C. Then, the mixture was washed with ethanol and distilled water and dried for 24 hours at 120 °C.

Synthesis of Zirconium Oxide

In a typical synthesis, Zirconium oxide is synthesized via hydrothermal method. 2.6g of Zr(NO₃)₄ and 0.24g of NaOH were dissolved in 70ml of water. It was stirred continuously for half an hour at room temperature[7]. The mixture was transferred into Teflon lined stainless steel autoclave and maintained at 120°C for 12h. The product was washed with water and ethanol to remove unwanted impurities and dehydrated at 80°C. The resultant material was annealed at 400°C for 5h in a muffle furnace.

Synthesis of Cobalt Zirconium Oxide

2.8g of CoCl₂.2H₂O and 0.6g of NaOH were dissolved in water and 2.7g of Zr(NO₃)₄ was added slowly. The solution was stirred continuously for half an hour at room temperature. The obtained mixture was transferred into Teflon lined stainless steel autoclave and maintained at 120°C for 12hrs. The product was washed with water and ethanol, removed to remaining ions, and dehydrated at 80°C in air. The resulting powder was annealed at 450°C for 5hrs in a muffle furnace [8].

Synthesis of rGO/CoZrO₂ Nanocomposite

30mg of rGO was sonicated for 10 minutes in which, 2.8g of CoCl₂.2H₂O, 2.7g Zr(NO₃)₄ and 0.6g of NaOH were added slowly. The solution was stirred continuously for 30 minutes at room temperature. The obtained mixture was transferred into a Teflon-lined stainless-steel autoclave and maintained at 120°C for 12 hrs. The resultant product was washed with ethanol and water and dehydrated at 80°C in air and the resulting sample was annealed at 450°C for 5 h in a muffle furnace [9].

Synthesis of rGO/Nd₂Zr₂O₇ Nanocomposite

2.7g of Zr(NO₃)₄, 0.2g of NaOH and 2.3g of Nd(NO₃)₃.6H₂O, were added and the solution was stirred continuously for 30 minutes at room temperature. 30mg of rGO was sonicated for 10 minutes and the solution was added into the beaker. The obtained mixture was transferred into a Teflon-lined stainless-steel autoclave and maintained at 120°C for 12 hrs. The resultant product was washed with ethanol and water and dried at 80°C in air and the resulting product was annealed at 450°C for 5 h in a muffle furnace [10].

Results and Discussion

XRD Analysis

The XRD patterns of the prepared samples after calcination at 500°C and the observed diffraction peaks at 2θ values of rGO present in the reflection planes of (002) and (100). ZrO₂ nanoparticle were found in the planes of (111), (002), (112) and (121), respectively (**JCPDS Card No. 89-4768**). CoZrO₃ composite are ascribed to the reflection plane of (111), (311), (222), (400) and (112), it is well matched with **JCPDS Card No. 14-0612**. Nd₂Zr₂O₇ composite are ascribed to the reflection plane of (001), (321), (400), (112) and (121) and it is well matched with **JCPDS Card No. 78-1618**. These phenomena indicate that the formation of rGO/CoZrO₂ and rGO/Nd₂Zr₂O₇ nanoparticles began at the calcination temperature of about 450°C [11]. Peaks are not detected in other phases, indicating the high purity of the products shown in **Fig.1**. The crystallite size of rGO/CoZrO₂ and rGO/Nd₂Zr₂O₇ nanocomposites was calculated using Debye–Scherrer formula (Equation 1) and the values are presented in **Table 1**.

Debye–Scherrer's equation

$$\text{Crystalline size (D)} = \frac{0.9\lambda}{\beta \cos\theta} \quad \text{----- (1)}$$

Where λ is the wavelength (λ = 1.5406 Å (Cu Kα)), β is the full width half maximum (FWHM) and θ is the diffraction angle.

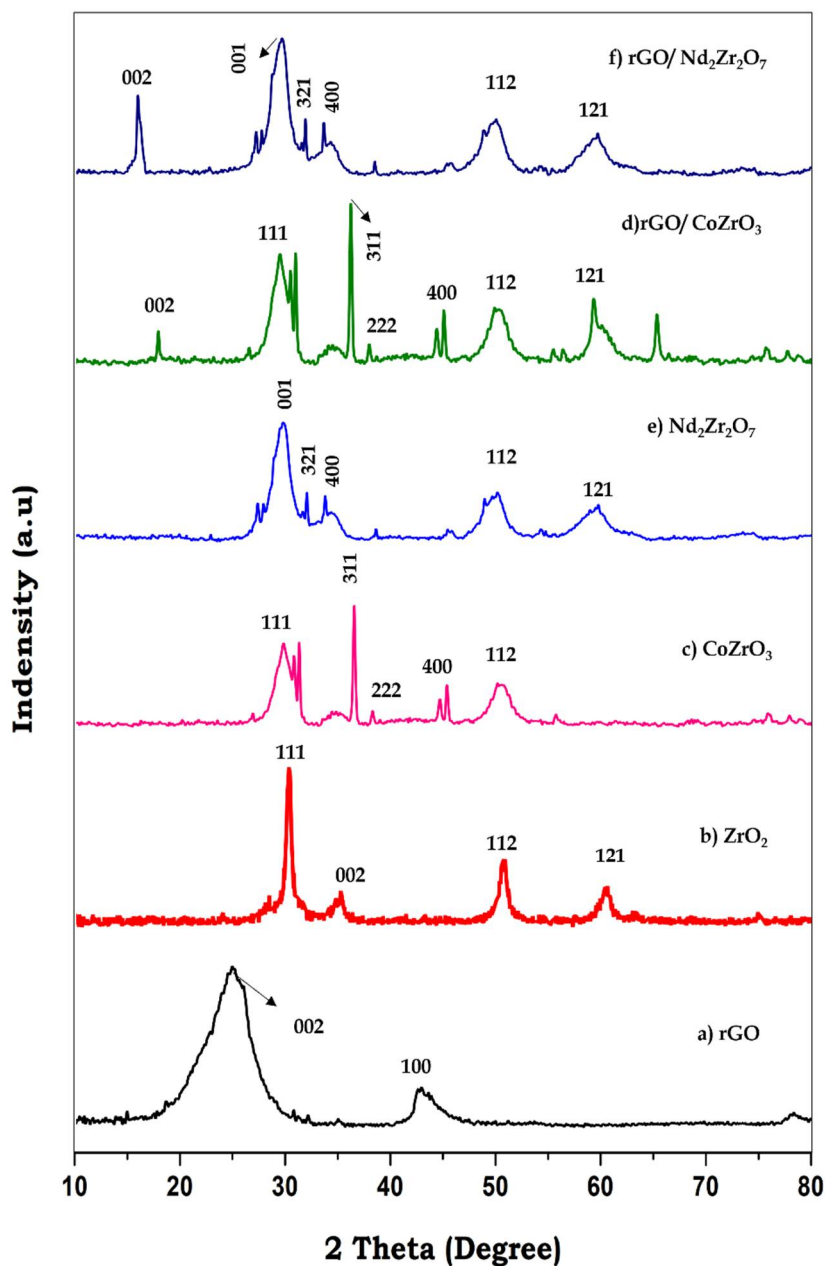


Fig.1 XRD spectra of (a) rGO, (b) ZrO_2 , (c) $CoZrO_3$, (d) $Nd_2Zr_2O_7$, (e) $rGO/CoZrO_3$ and (f) $rGO/Nd_2Zr_2O_7$

Table.1. Crystalline size of rGO, ZrO_2 , $CoZrO_3$, $Nd_2Zr_2O_7$, $rGO/CoZrO_3$ and $rGO/Nd_2Zr_2O_7$

S.No	Sample	Crystalline Size(nm)
1.	rGO	26.5
2.	ZrO_2	30.2
3.	$CoZrO_3$	38.7
4.	$Nd_2Zr_2O_7$	44.0
5.	$rGO/CoZrO_3$	40.3
6.	$rGO/Nd_2Zr_2O_7$	48.6

FT-IR Spectrum of rGO, ZrO_2 , $CoZrO_3$, $Nd_2Zr_2O_7$, $rGO/CoZrO_3$ and $rGO/Nd_2Zr_2O_7$

The FT-IR technique is a strong tool to analyze the different functional groups found in graphene oxide, including functional groups involving oxygen. FT-IR spectra of rGO, ZrO_2 , $CoZrO_3$, $rGO/CoZrO_3$ and $rGO/Nd_2Zr_2O_7$ are shown in **Fig.2**. The FT-IR spectrum of rGO is shown in **Fig.2a**. The stretching vibration

peaks at 601 cm^{-1} due to the stretching mode of the Zr-O band and H-O-H band observed at 3388 cm^{-1} for ZrO_2 (**Fig.2b**). Metal-oxygen stretching vibration peaks of the CoZrO_3 appeared at 526 and 558 cm^{-1} and the H-O-H band appeared at 3462 cm^{-1} as show in **Fig.2c** and is good agreement with the reported values[12]. The metal-oxygen and H-O-H banding of $\text{Nd}_2\text{Zr}_2\text{O}_7$ is appeared at 538 , 580 and 3586 cm^{-1} respectively. In the $\text{rGO}/\text{CoZrO}_3$ composite band at 586 and 680 cm^{-1} due to the metal-oxygen stretching vibration and H-O-H band appeared at 3462 cm^{-1} , whereas in $\text{rGO}/\text{Nd}_2\text{Zr}_2\text{O}_7$ composite, the metal-oxygen band appeared at 556 cm^{-1} and this co-existence may be significant, since it prevents the combination of charge carriers and also induces a synergistic effect to enhance the catalytic and microbial activity of the nanocomposites.

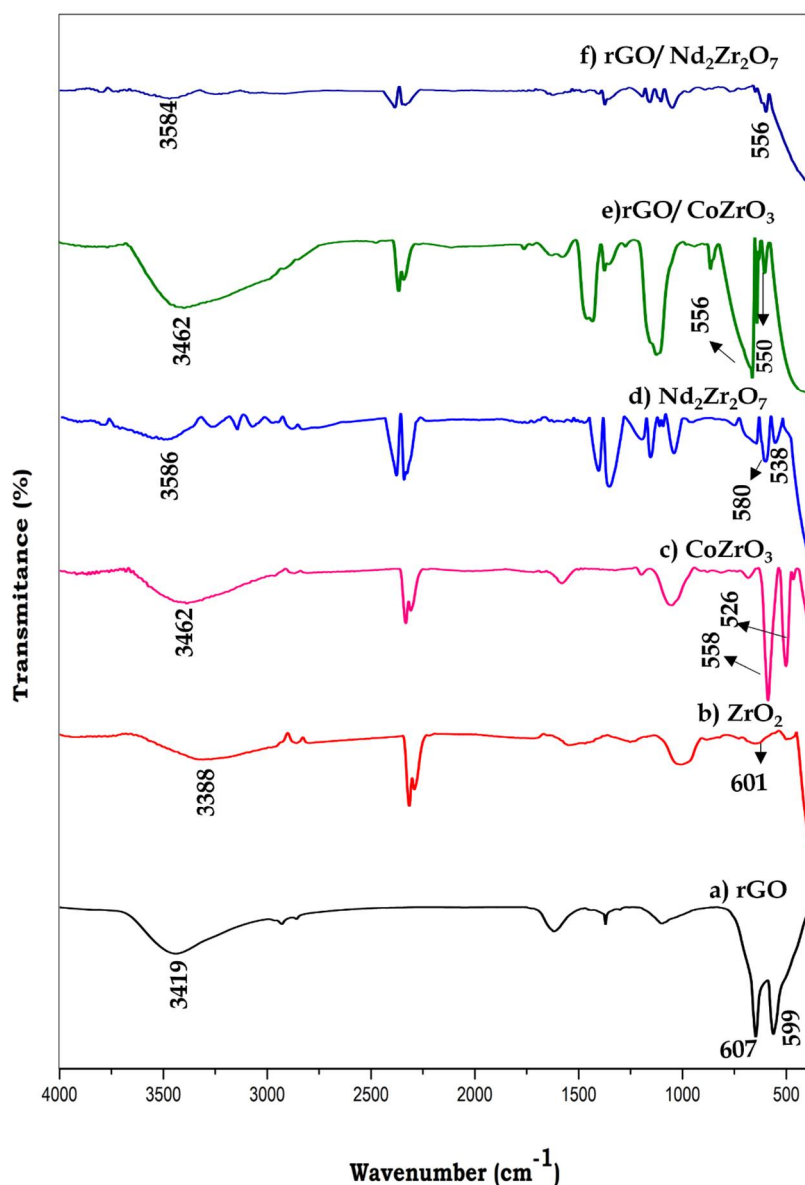


Fig. 2. FT-IR Spectrum of (a) rGO, (b) ZrO_2 , (c) CoZrO_3 , (d) $\text{Nd}_2\text{Zr}_2\text{O}_7$, (e) $\text{rGO}/\text{CoZrO}_3$ and (f) $\text{rGO}/\text{Nd}_2\text{Zr}_2\text{O}_7$

Morphology Analysis

The surface morphology of the as prepared rGO, ZrO_2 , CoZrO_3 , $\text{Nd}_2\text{Zr}_2\text{O}_7$, $\text{rGO}/\text{CoZrO}_3$ and $\text{rGO}/\text{Nd}_2\text{Zr}_2\text{O}_7$ was analyzed using SEM micrographs and presented in **Fig.3a-f**. The SEM images of rGO exhibited a sheet-like structure **Fig.3a** [13]. The surface morphology of ZrO_2 shows different shapes of ZrO_2 are agglomerated, as shown in **Fig.3b**[13]. Further, the CoZrO_3 and $\text{Nd}_2\text{Zr}_2\text{O}_7$ nanoparticles exhibited as aggregated flakes (**Fig.3c** and **Fig.3d**). Interestingly, in the $\text{rGO}/\text{CoZrO}_3$ and $\text{rGO}/\text{Nd}_2\text{Zr}_2\text{O}_7$ nanocomposites, the different shaped flakes of CoZrO_3 and $\text{Nd}_2\text{Zr}_2\text{O}_7$ nanoparticles are distributed on the rGO surface in different directions **Fig.3e** and **Fig.3f**.

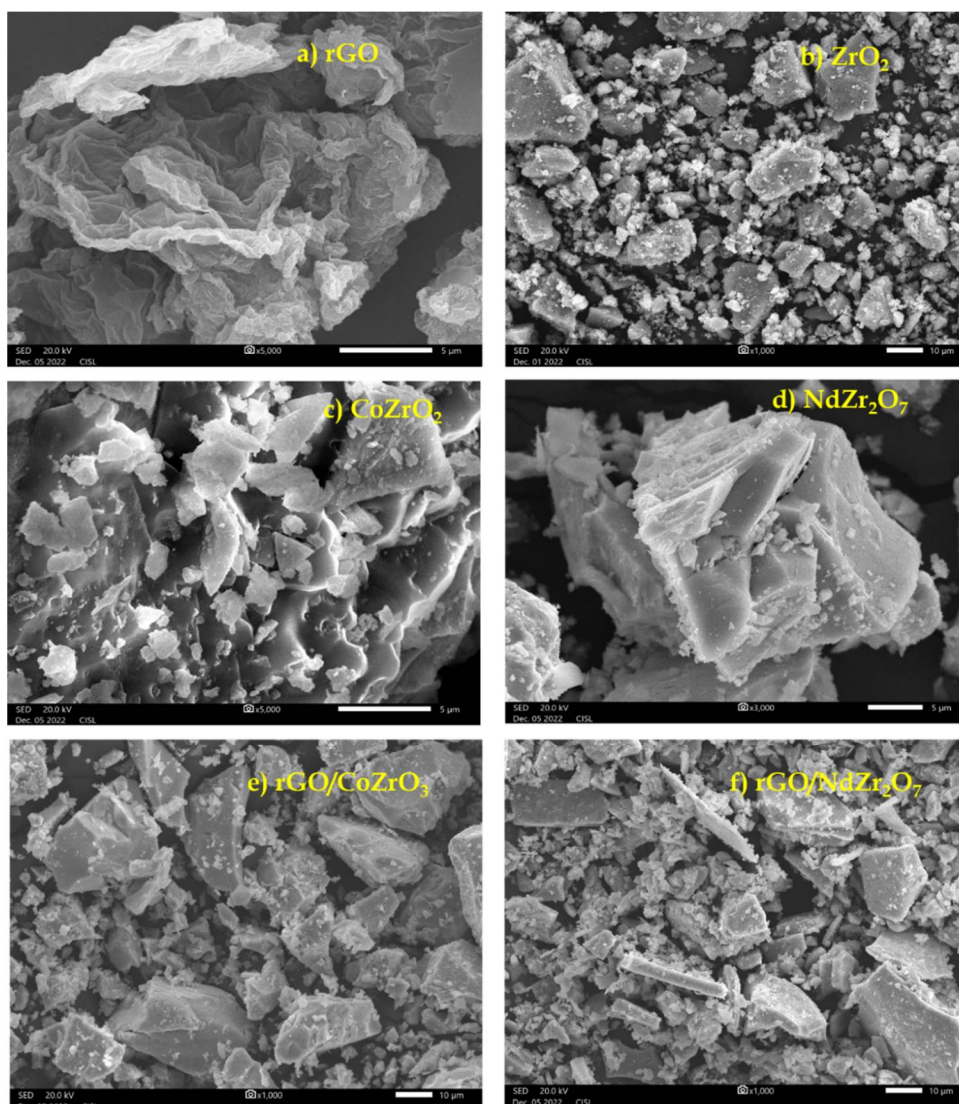


Fig. 3. Morphology analysis of (a) rGO, (b) ZrO_2 , (c) $CoZrO_3$, (d) $Nd_2Zr_2O_7$, (e) $rGO/CoZrO_3$ and (f) $rGO/Nd_2Zr_2O_7$

XPS Analysis

XPS analysis was used to investigate the surface elemental composition and their exact ionic states. **Fig. 4a** portrayed the over-all XPS survey spectrum of as prepared $rGO/CoZrO_3$ which clearly revealed that the appearance of Zr, Co, O and C elements. The high magnification deconvoluted XPS spectra of $Co2p$ was shown in **Fig. 4b**. The binding energy peaks at 781.3 eV and 796.2 eV are ascribed to the $Co2p_{3/2}$ and $Co2p_{1/2}$ spin orbits, respectively. Also, the binding energy of $Zr3d$ illustrates Peaks values of 183.2 and 185.5 eV in **Fig. 4c** related to the $Zr3d_{5/2}$ and $Zr3d_{3/2}$, respectively [2]. From the **Fig. 4d** the $O1s$ peaks displayed the two characteristic peaks at the binding energies of 531.0 and 537.3 eV related presence of lattice oxygen, adsorbed and chemisorbed oxygen molecules, respectively [14]. **Fig. 4e** shows the deconvoluted $C-1s$ spectra of $rGO/CoZrO_3$ nanocomposites, it shows the $C-1s$ peak appears at 285.3 eV due to carbon sp^2 C=C [15]. This result suggests that the rGO was successfully anchored with the $CoZrO_3$ in the $rGO/CoZrO_3$ nanocomposite.

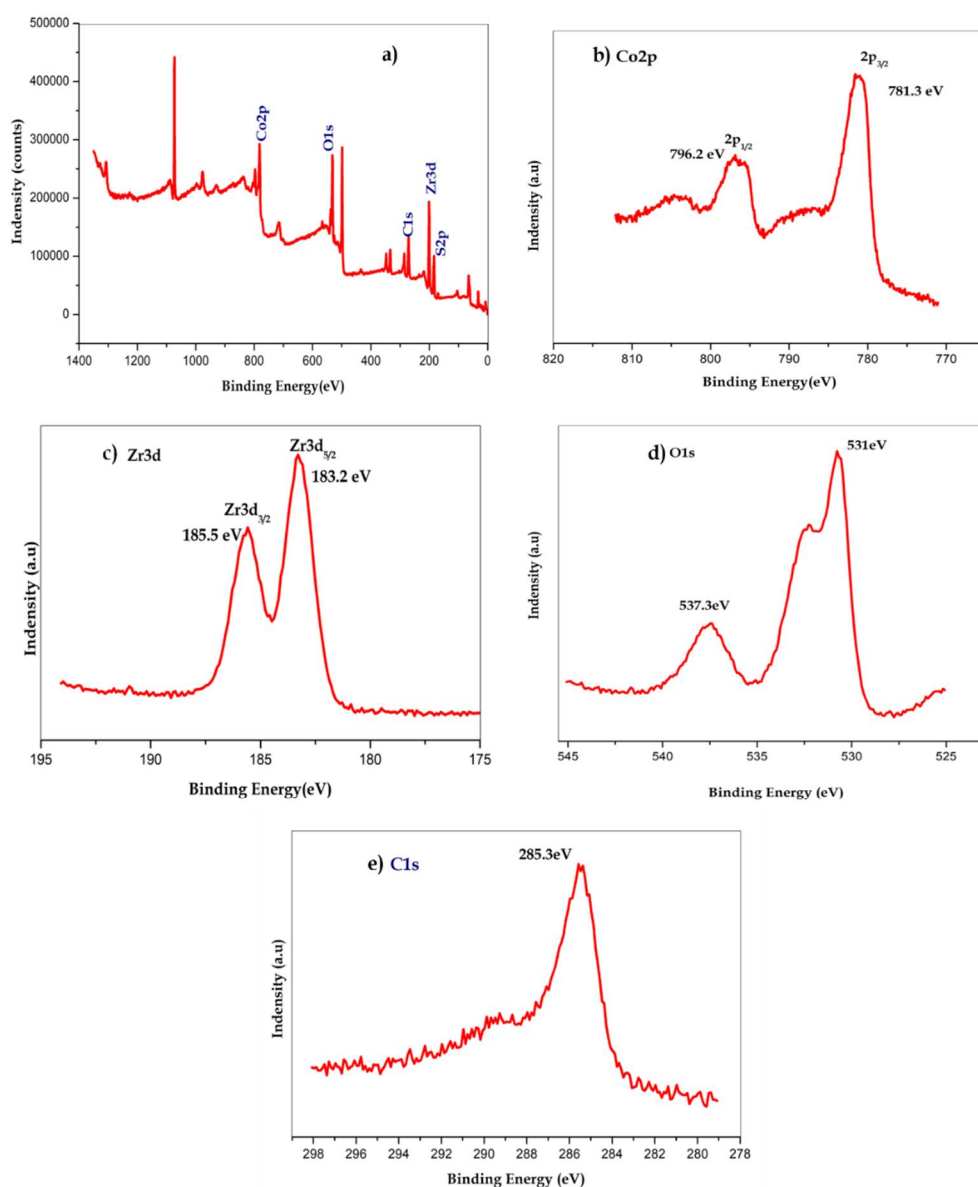


Fig. 4. XPS spectra of rGO/ CoZrO₃ nanocomposite, (a) Survey spectrum, (b) Co2p core spectrum, (c) Zr3d core spectrum, (d) O1s core spectrum and (e) C1s core spectrum

The XPS spectra of rGO/NdZr₂O₇ nanocomposite as from **Fig. 5** shows the XPS spectra of Nd3d, Zr3d, O1s and C1s. **Fig. 5a**, the rGO/NdZr₂O₇ nanocomposite was shows the Nd3d, Zr3d, O1s and C1s states alone presented in the samples. **Fig. 5b** shows the deconvoluted XPS spectrum of Nd3d exhibits the energy levels of 983.3 and 1006.3 eV which corresponds to the binding energies of Nd3d_{5/2} and Nd3d_{3/2}, respectively [16].

Also, the binding energy of Zr3d illustrates peaks values of 184.1eV (**Fig. 5c**) related to the Zr3d_{5/2} and Zr3d_{3/2}, respectively [17]. The O1s core level spectrum of rGO/NdZr₂O₇ nanocomposite (**Fig. 5d**) displayed a band at 532.7 eV due to Nd-O linkages in the nanocomposite. **Fig. 5e** shows the C1s spectra of rGO/NdZr₂O₇ nanocomposites, it shows the C1s peak appears at 285.5 eV due to carbon sp² C=C. Based on XRD and XPS results, the rGO was found to be incorporated into NdZr₂O₇ lattice [7].

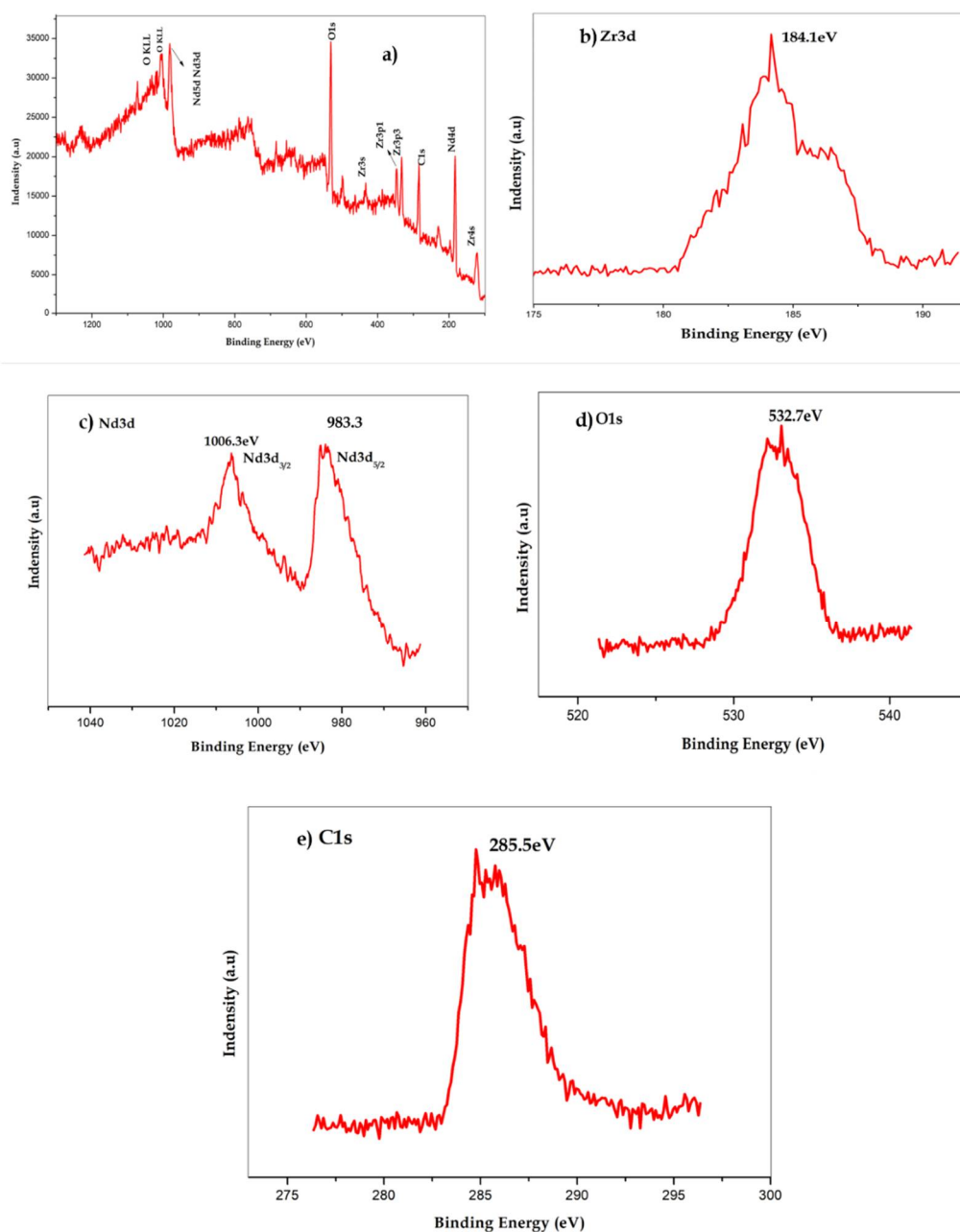


Fig. 5 XPS spectra of rGO/NdZr₂O₇ nanocomposite, (a) Survey spectrum, (b) Nd3d core spectrum, (c) Zr3d core spectrum, (d) O1s core spectrum and (e) C1s core spectrum

UV - DRS Analysis

UV – diffuse reflectance spectroscopy of rGO/CoZrO₃ and rGO/Nd₂Zr₂O₇ nanocomposites are shown in **Fig.6** and it is illustrated that pure ZrO nanoparticles had significant UV absorption edge observed at 200 to 800nm. But the UV absorption of other samples shifted towards higher wavelength side[18]. The changes in the absorption edges show the changes in the band structure. Further, the bandgap of samples is determined by Kubelka – Munk function (equation-2).

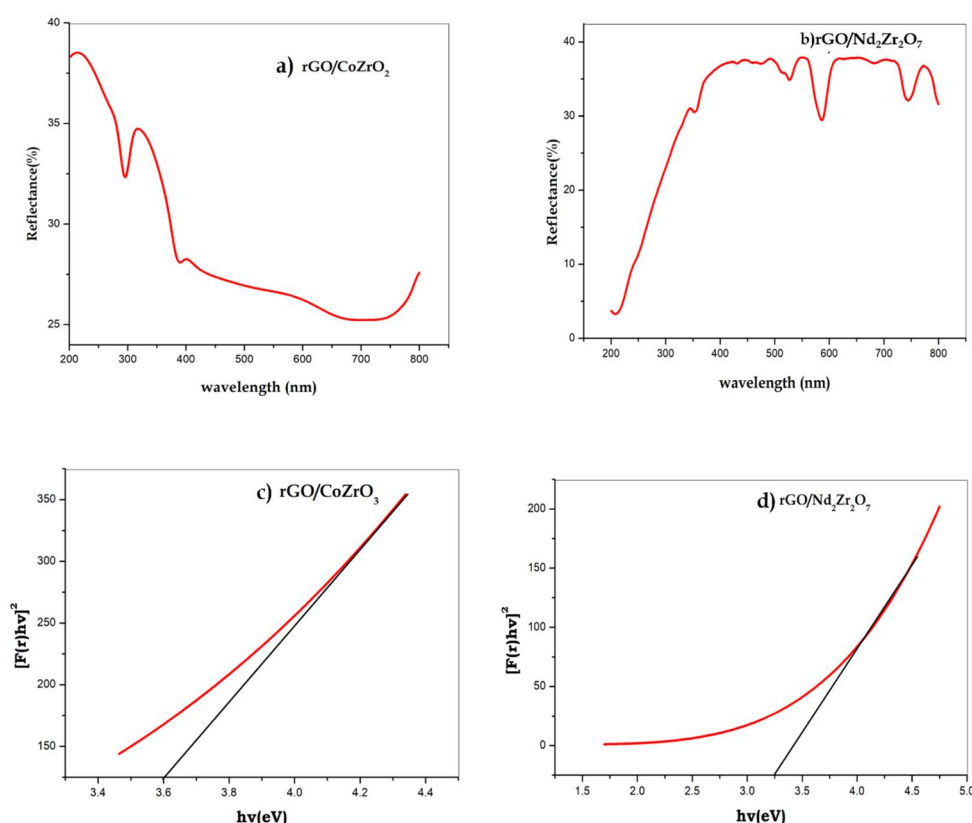


Fig. 6 UV-DRS Image of (a) rGO/CoZrO₃, (b) rGO/Nd₂Zr₂O₇ and (c) Tauc Plot of rGO/CoZrO₃ and (d) Tauc Plot of rGO/Nd₂Zr₂O₇

$$\alpha h\nu = A (h\nu - E_g)^n \text{ ----- (2)}$$

Here, α is the absorption coefficient and $h\nu$ is the incident photon energy. As shown in **Fig.6**, the bandgap energies are estimated from the intercept of the tangents. The band gap of prepared rGO/CoZrO₃ and rGO/Nd₂Zr₂O₇ nanocomposites were found to be 3.6 and 3.2 eV respectively. The presence of oxygen vacancies can create impurity level near the valance band, the rGO/ Nd₂Zr₂O₇ having lower band gap value and it is having more catalytic and antimicrobial activity compared to the rGO/ CoZrO₃ material[19].

Photocatalytic activity

The photocatalytic activities of the synthesized rGO/CoZrO₃ and rGO/ Nd₂Zr₂O₇ nanocomposite were evaluated by the degradation of methylene blue (MB) dye (**Fig.7**). **Fig.7** shows the dye degradation using sunlight irradiation was carried out within 60 minutes. **Fig. 8** shows the rGO/CoZrO₃ and rGO/ Nd₂Zr₂O₇ nanocomposites degradation efficiency is 72.7 and 88.2% respectively. Hence, it was concluded that rGO/ Nd₂Zr₂O₇ nanocomposite has the appreciable photocatalytic degradation efficiency as compared to the pure rGO/CoZrO₃ nanocomposite [20]. According to the photocatalytic degradation results, rGO/Nd₂Zr₂O₇ was utilized as an eco-friendly catalyst for remediation of the environment and photocatalytic degradation.

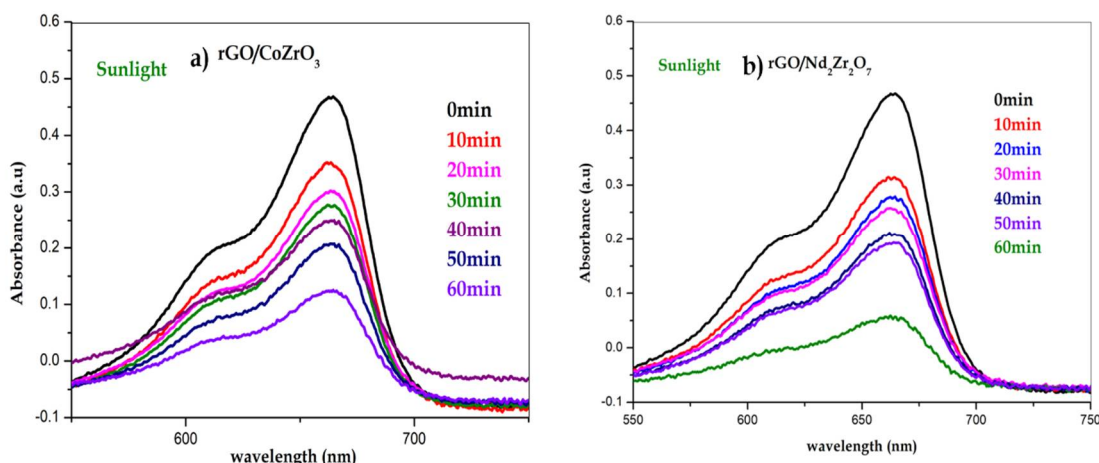


Fig. 7. Photocatalytic activity of (a) rGO/CoZrO₃ and (b) rGO/Nd₂Zr₂O₇

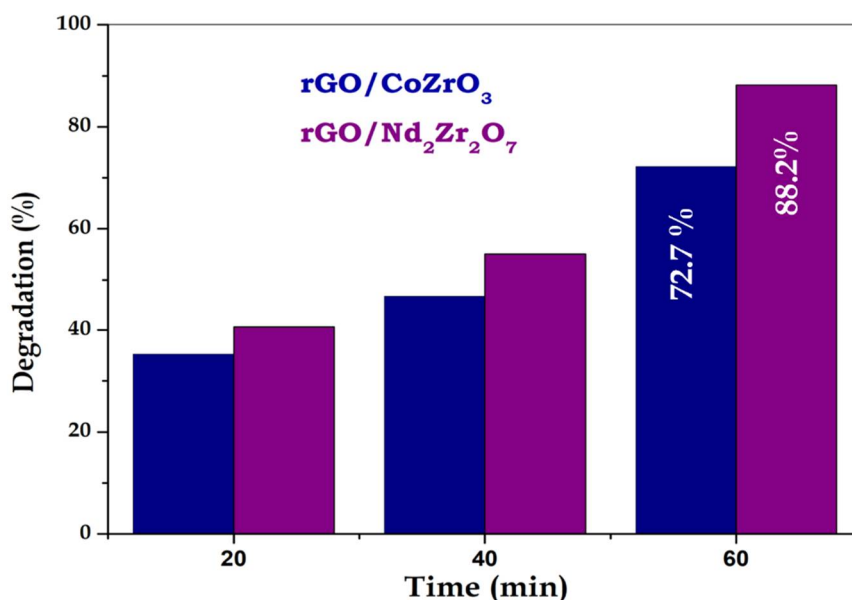


Fig. 8. Degradation efficiency of (a) rGO/CoZrO₃ and (b) of rGO/Nd₂Zr₂O₇

Photocatalytic mechanism

According to the actual mechanism of methylene blue dye degradation, when the rGO/CoZrO₃ and rGO/Nd₂Zr₂O₇ nanocomposites is irradiated with light energy greater than or equivalent to its band gap energy, conduction band electrons (e⁻) and valence band holes (h⁺) are generated. The generation of hydroxyl radicals mediates the oxidation of organic molecules, whereas the synthesis of superoxide radicals mediates the reduction and oxidation reactions. Fig.9 depicts a schematic illustration of the degradation mechanism. The notion that the hydroxyl radical form is to blame for the oxidation route of chemical compounds initiated by heterogeneous photocatalysis [21]. The dye may be reduced or the photogenerated electrons could react with electron acceptors such O₂ adsorbed on the rGO surface or dissolved in water, reducing it to superoxide radical anion ·O₂⁻. The photogenerated holes can oxidize organic molecules by interacting with ·OH or H₂O to produce ·OH radicals. Because the ·OH radical is such a potent oxidizing agent, it can oxidize most MB into non-toxic end products such as CO₂, H₂O and mineralized products.

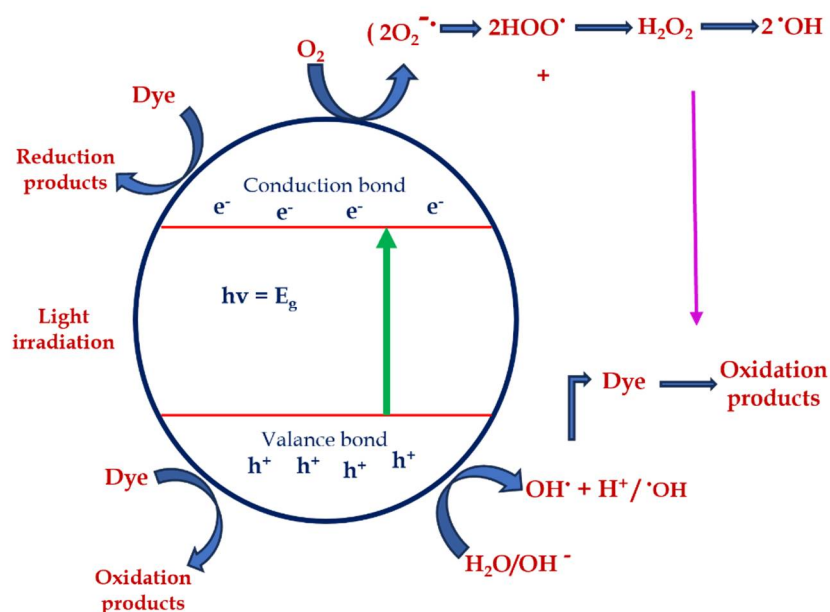


Fig.9 Schematic illustration of the Photocatalytic degradation mechanism

Photocatalytic reaction kinetics

The photodegradation rate of methylene blue (MB) dye with the nanocatalysts (20mg) was determined at various time intervals. A linear correlation was detected between $\ln(C_0/C_t)$ and reaction time t (Fig.10), showing that the photocatalytic degradation of methylene blue (MB) dye by rGO/ CoZrO₃ and rGO/ Nd₂Zr₂O₇ follows a pseudo-first order kinetic model (Eq-3).

$$\ln(C_0/C_t) = -kt \dots\dots (3)$$

Where "Co" denotes the initial concentration (mmol/L), "Ct" is the dye's instantaneous concentration at different illumination intervals, and k denotes the apparent rate constant. The rate constant for photodegradation of methylene blue (MB) dye under sunlight irradiation of rGO/CoZrO₃ and rGO/Nd₂Zr₂O₇ is given in Fig.10, and the observed rate constant suggested that the rGO/ Nd₂Zr₂O₇ had a higher rate constant ($1.65 \times 10^{-3} \text{ min}^{-1}$) when exposed to sunlight.

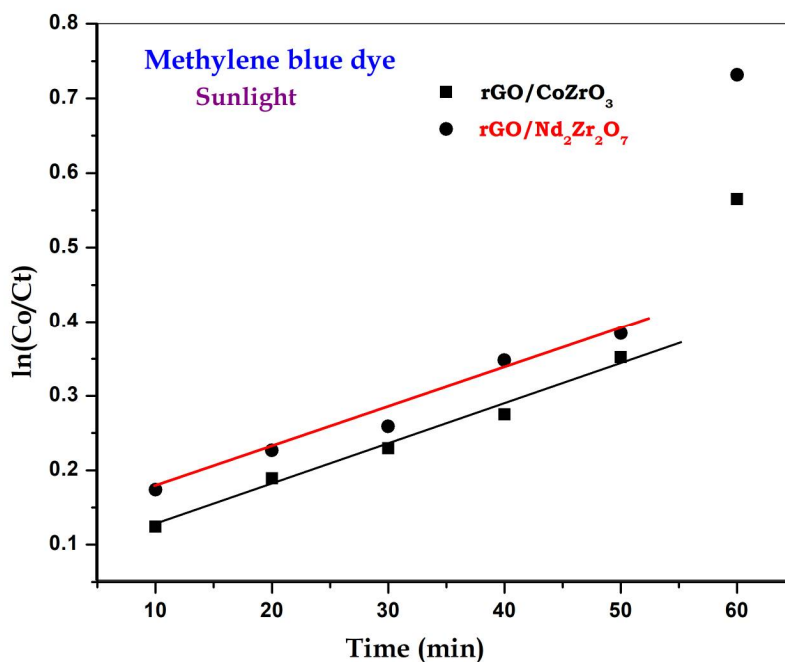


Fig.10. Pseudo-first order plot of the prepared nanocomposite under sunlight irradiation

Antibacterial activity

Procedure

The antibacterial activity of the synthesized nanocomposites were tested against the bacterial pathogens by agar well diffusion method. For this, bacterial pathogens were inoculated in nutrient broth and incubated for 12 h before predicting antibacterial assay. All the bacterial strains were individually spread on the Muller Hinton agar plates. Wells were made in the plates at 6mm by using cork borer. Samples are dissolved in DMSO. The different concentrations (25 µl to 100 µl) of samples added on the wells and incubated for 37°C at 24 hours. Chloramphenicol is used as a positive control. The assay was carried out in triplicates[22]. The zone of inhibition was measured in mm after the completion of the incubation period.

Results of antibacterial activity

Antibacterial activity of the nanocomposite samples of rGO/CoZrO₃ and of rGO/Nd₂Zr₂O₇ were tested against four clinical bacterial pathogens: Gram-positive- *Staphylococcus aureus*, *Streptococcus pneumoniae* and Gram-negative - *Escherichia coli*, *Klebsiella pneumoniae*. The different concentrations (25 µl to 100 µl) of samples were used for antibacterial activity.

The rGO/CoZrO₃ nanocomposite showing the maximum zone of inhibition was observed against *Streptococcus pneumoniae* (16 mm) followed by *Escherichia coli* (15 mm), *Staphylococcus aureus* (14 mm) and minimum zone of inhibition against *Klebsiella pneumoniae* is 13 mm at 100 µl of concentration[23].

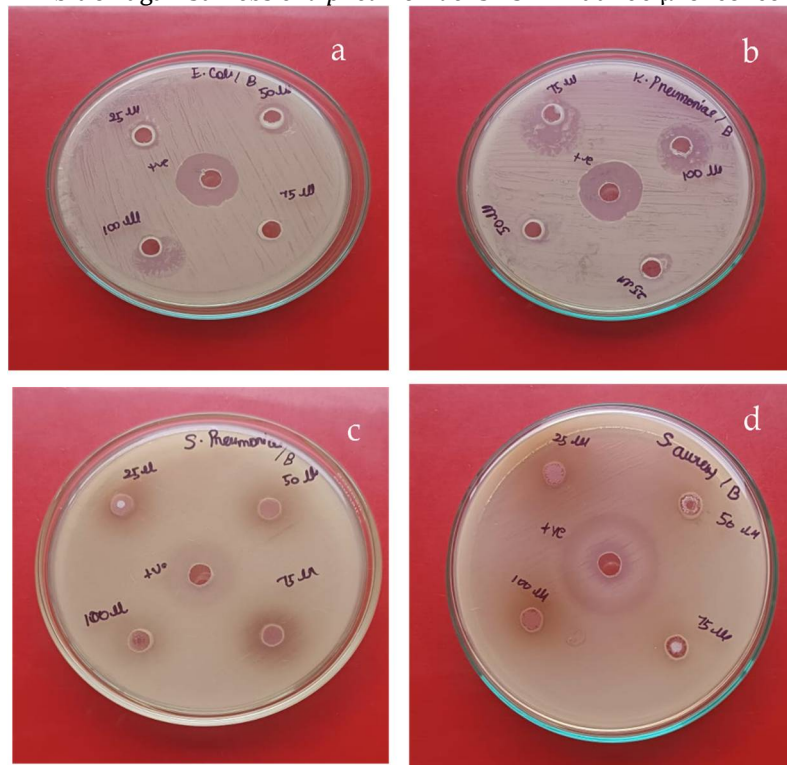


Fig.11 Antibacterial activity of rGO/CoZrO₃ nanocomposite

Table:2 Antibacterial activity of rGO/CoZrO₃ nanocomposite

S. No	Bacterial Pathogens	Zone of Inhibition (mm)				
		25µl	50 µl	75 µl	100 µl	Standard (+Ve)
1	<i>Staphylococcus aureus</i>	8	9	11	14	13
2	<i>Streptococcus pneumoniae</i>	10	13	15	16	25
3	<i>Escherichia coli</i>	9	11	13	15	20
4	<i>Klebsiella pneumoniae</i>	7	9	12	13	23

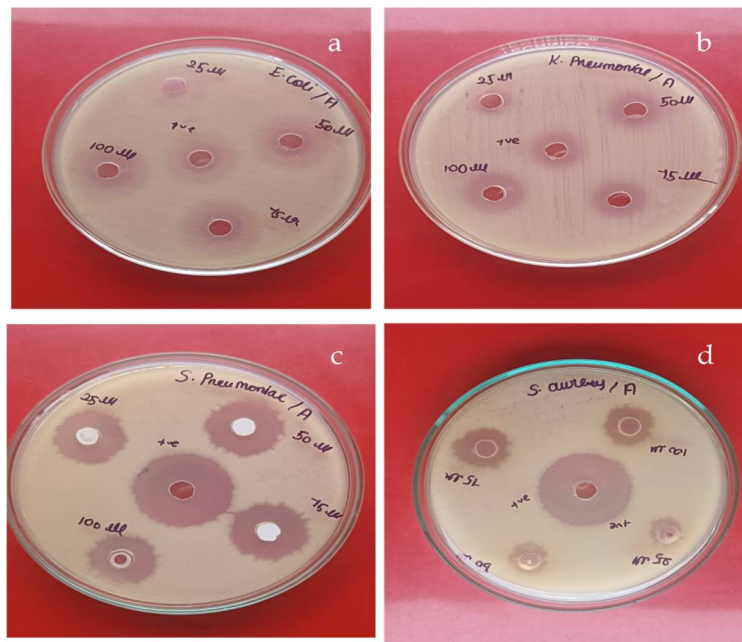


Fig.12. Antibacterial activity of nanocomposite rGO/ Nd₂Zr₂O₇

The nanocomposites of rGO/ Nd₂Zr₂O₇ showing the maximum zone of inhibition was observed against *Streptococcus pneumoniae* (25 mm) followed by *Escherichia coli* (22 mm), *Staphylococcus aureus* (19 mm) and minimum zone of inhibition against *Klebsiella pneumoniae* (18 mm) at 100 µl of concentration [24].

Table 3. Antibacterial activity of rGO/ Nd₂Zr₂O₇ nanocomposite

S.No	Bacterial Pathogens	Zone of Inhibition (mm)				
		25 µl	50 µl	75 µl	100 µl	Standard (+Ve)
1	<i>Staphylococcus aureus</i>	8	10	12	19	30
2	<i>Streptococcus pneumoniae</i>	26	21	23	25	29
3	<i>Escherichia coli</i>	16	18	20	22	23
4	<i>Klebsiella pneumoniae</i>	10	12	14	18	17

The synthesized nanocomposite rGO/CoZrO₃ and rGO/Nd₂Zr₂O₇ were screened against four bacterial pathogens for antibacterial activity by agar well diffusion method. In this antibacterial activity, the composite of rGO/Nd₂Zr₂O₇ sample showed highest antibacterial activity against all the clinical bacterial pathogens.

CONCLUSION

The hydrothermal approach was employed to synthesize the nanomaterials viz., rGO, ZrO₂, CoZrO₃, rGO/Nd₂Zr₂O₇ and rGO/CoZrO₂. The size of the synthesized nanomaterials rGO, ZrO₂, CoZrO₃, Nd₂Zr₂O₇, rGO/CoZrO₃ and rGO/ Nd₂Zr₂O₇ were found to be 26.5, 30.2, 38.7, 40.3, 44.0 and 48.6 nm respectively with the agglomerated structures. Kubelka-Munk function plot scrutinized that the band gap of rGO/CoZrO₃ and rGO/ Nd₂Zr₂O₇ was found to be 3.6 and 3.2 eV, respectively. The rGO/ Nd₂Zr₂O₇ nanocomposite having a high degradation property (88.2%) with MB dye compared to rGO/CoZrO₃ (72.7%). The antibacterial study revealed that the prepared nanomaterials might be useful as a good antimicrobial agent.

ACKNOWLEDGEMENTS

Authors are thankful to the Department of Chemistry, Annamalai University and RUSA.2.0 project for providing necessary funding to carry out this research work.

REFERENCES

- Sahithya K. Karthika K. (2022). Green Synthesis of Silver Nanoparticles using Marine Seaweed *Acetabularia acetabulum* and their Activity as MMT-Ag Nanocomposites towards Antifouling Applications. *Research Journal of Pharmacy and Technology*. ;15(12):5397-404.
- Li P. Guo M. Wang Q. Li Z. Wang C. Chen N. Wang CC. Wan C. Chen S. (2019). Controllable synthesis of cerium zirconium oxide nanocomposites and their application for photocatalytic degradation of sulfonamides. *Applied Catalysis B: Environmental*. 259:118107.

3. Riyal I. Badoni A. Kalura SS. Mishra K. Sharma H. Gambhir L. Dwivedi C. (2022). Antimicrobial activity of synthesized graphene oxide-selenium nanocomposites: A mechanistic insight. *Environmental Science and Pollution Research*. 13:1-9.
4. Ismail NA. Shameli K. Mohamad Sukri SN. Hara H. Teow SY. Moeini H. (2022). Sonochemical synthesis of a copper reduced graphene oxide nanocomposite using honey and evaluation of its antibacterial and cytotoxic activities. *Frontiers in Molecular Biosciences*. ;9.
5. Prema D. Prakash J. Vignesh S. Veluchamy P. Ramachandran C. Samal DB. Oh DH. Sahabudeen S. Devanand Venkatasubbu G. (2020). Mechanism of inhibition of graphene oxide/zinc oxide nanocomposite against wound infection causing pathogens. *Applied Nanoscience*. ;10(3):827-49.
6. Sahoo JK. Paikra SK. Baliarsingh A. Panda D. Rath S. Mishra M. Sahoo H. (2020). Surface functionalization of graphene oxide using amino silane magnetic nanocomposite for Chromium (VI) removal and bacterial treatment. *Nano Express*. 30;1(1):010062.
7. Al-Zaqri N. Muthuvel A. Jothibas M. Alsalmeh A. Alharthi FA. Mohana V. (2021). Biosynthesis of zirconium oxide nanoparticles using *Wrightia tinctoria* leaf extract: Characterization, photocatalytic degradation and antibacterial activities. *Inorganic Chemistry Communications*. 1; 127:108507.
8. Sharmila G C. Muthukumar, K. Sandiya S. Santhiya R. Sakthi Pradeep N. Manoj Kumar N. Suriyanarayanan M. Thirumarimurugan (2018). "Biosynthesis, Characterization, and Antibacterial Activity of Zinc Oxide Nanoparticles Derived from *Bauhinia tomentosa* Leaf Extract, *Journal of Nanostructure Chemistry*. 8; 293–2993.
9. Rani P. Siril P.F. Srivastava R. (2017). Cu nanoparticles decorated Cu organic framework based efficient and reusable heterogeneous catalyst for coupling reactions, *Molecular Catalyst* 433; 100–110.
10. Alharthi F.A. Alghamdi A.A. Alotman. A.A. Almarhoon Z.M. Alsulaiman M.F. Al-Zaqri N. Green Synthesis of ZnO Nanostructures Using *Salvadora persica* Leaf Extract: Applications for Photocatalytic Degradation of Methylene Blue Dye, *Crystals* 10 (2020) 441.
11. Hu C. Sun J. Long C. Wu L. Zhou C. Zhang X. (2019). Synthesis of nano zirconium oxide and its application in dentistry, *Nanotechnology Review* 8; 396–404.
12. Eshed M. Pol S. Gedanken A. Balasubramanian M. (2011). Zirconium nanoparticles prepared by the reduction of zirconium oxide using the RAPET method, *Bulletin Journal of Nanotechnology*. 2 :198–203.
13. Panahi D. Dastan N.B. Chaure, Characterization of Zirconia Nanoparticles Grown by Sol-Gel Method, *Advanced Science Letters* 22 (2016) 941–944.
14. Liang L. Jiang X. Liu G. Deng Z. Zhuang J. Li F. Li Y. Characterization and synthesis of pure ZrO₂ nanopowders via sonochemical method, *Materials Research Bulletin* 38 (2003) 161–168.
15. Wang J. Yin W. He X. Wang Q. Guo M. Chen S. (2016). Good Biocompatibility and Sintering Properties of Zirconia Nanoparticles Synthesized via Vapor-phase Hydrolysis, *Scientific Reports* 6.78-84
16. Bumajdad A. Nazeer A.A. Al F. Sagheer S. Nahar M.I. Zaki Controlled Synthesis of ZrO₂ Nanoparticles with Tailored Size, Morphology and Crystal Phases via Organic/Inorganic Hybrid Films, *Scientific Reports* (2018) 8.
17. Tok F. Boey C. Du S. Wong B.K. (2006). Flame spray synthesis of ZrO₂ nano-particles using liquid precursors, *Materials Science and Engineering B* 130; 114–119.
18. Liang J. Deng Z. Jiang X. Li F. Li Y. (2002). Photoluminescence of Tetragonal ZrO₂ Nanoparticles Synthesized by Microwave Irradiation, *Inorganic Chemistry* 41; 3602–3604.
19. Vinu D. Govindaraju D.K. Vasantharaja R. Amreen Nisa S. Kannan M. Vijai Anand K. (2020). Biogenic zinc oxide, copper oxide and selenium nanoparticles: preparation, characterization and their anti-bacterial activity against *Vibrio parahaemolyticus*, *Journal of Nanostructure in Chemistry* :100-104
20. Omidi S. Sedaghat S. Tahvildari K. Derakhshi P. Motiee F. Biosynthesis of silver nanocomposite with Tarragon leaf extract and assessment of antibacterial activity, *Journal of Nanostructure in Chemistry* 8 (2018) 171–178.
21. Muthuvel A. Jothibas M. Manoharan C.(2020). Synthesis of copper oxide nanoparticles by chemical and biogenic methods: photocatalytic degradation and in vitro antioxidant activity, *Nanotechnology for Environmental Engineering* 5: 20-24.
22. Shinde H.M. Bhosale T.T. Gavade N.L. Babar S.B. Kamble R.J. Shirke B.S. Garadkar K. M. (2018). Biosynthesis of ZrO₂ nanoparticles from *Ficus benghalensis* leaf extract for photocatalytic activity, *The Journal of Materials Science: Materials in Electronics* 29 14055–14064.
23. Shanthi S. Sri S. Nisha T.(2016). Green Synthesis of Zirconium Dioxide (ZrO₂) Nano Particles Using *Acalypha indica* Leaf Extract, *International Journal of Applied Science and Engineering* 3 :90-97.
24. Gowri S. Gandhi R.R. Senthil S. Sundrarajan M. (2015). Effect of Calcination Temperature on *Nyctanthes* Plant Mediated Zirconia Nanoparticles; Optical and Antibacterial Activity for Optimized Zirconia, *Journal of Bio nanoscience*. 9: 181–189.

CITATION OF THIS ARTICLE

Mathivanan N, Krishnasamy K. Synthesis, Characterization of rGO/CoZrO₃ and rGO/Nd₂Zr₂O₇ nanocomposite for the application of Photocatalytic and Antimicrobial Activity. *Bull. Env. Pharmacol. Life Sci.*, Vol 12[10] September 2023: 204-216.